

Contents lists available at [ScienceDirect](http://ScienceDirect)

Physics Letters B

[www.elsevier.com/locate/physletb](http://www.elsevier.com/locate/physletb)

## Study of double pion photoproduction on the deuteron

K. Hirose<sup>a,\*</sup>, M. Ejima<sup>a</sup>, T. Fujibayashi<sup>a</sup>, Y. Fujii<sup>a</sup>, K. Futatsukawa<sup>a</sup>, O. Hashimoto<sup>a</sup>, T. Ishikawa<sup>b</sup>, S. Kameoka<sup>a</sup>, H. Kanda<sup>a</sup>, F. Kato<sup>a</sup>, S. Kinoshita<sup>a</sup>, T. Kinoshita<sup>b</sup>, T. Kon<sup>a</sup>, O. Konno<sup>c</sup>, K. Maeda<sup>a</sup>, A. Matsumura<sup>a</sup>, Y. Miura<sup>a</sup>, F. Miyahara<sup>b</sup>, H. Miyase<sup>a</sup>, T. Nakabayashi<sup>b,2</sup>, S.N. Nakamura<sup>a</sup>, H. Nomura<sup>a</sup>, K. Nonaka<sup>a</sup>, A. Ohtani<sup>a</sup>, Y. Okayasu<sup>a</sup>, M. Oyamada<sup>a</sup>, A. Sasaki<sup>d</sup>, H. Shimizu<sup>b</sup>, T. Takahashi<sup>a,3</sup>, T. Tamae<sup>b</sup>, H. Tamura<sup>a</sup>, T. Terasawa<sup>b</sup>, H. Tsubota<sup>a</sup>, K. Tsukada<sup>a,4</sup>, D. Uchida<sup>a</sup>, M. Ukai<sup>a,5</sup>, M. Wakamatsu<sup>a</sup>, T. Watanabe<sup>a,5</sup>, H. Yamauchi<sup>a</sup>, H. Yamazaki<sup>b</sup>, K. Yawata<sup>a</sup>

<sup>a</sup> Department of Physics, Tohoku University, Sendai, 980-8578, Japan<sup>b</sup> Laboratory of Nuclear Science, Tohoku University, Sendai, 982-0826, Japan<sup>c</sup> Ichinoseki National College of Technology, Ichinoseki 021-8511, Japan<sup>d</sup> Department of Electrical and Electronic Engineering, Akita University, Akita 010-8502, Japan

## ARTICLE INFO

## Article history:

Received 5 September 2007

Received in revised form 28 January 2009

Accepted 22 February 2009

Available online 26 February 2009

Editor: V. Metag

## PACS:

13.60.Le

25.20.Lj

## Keywords:

Nuclear reaction  $\gamma p \rightarrow p\pi^+\pi^-$  $\gamma d \rightarrow \Delta^{++}\Delta^-$  $E_\gamma$  from 0.8 to 1.1 GeV

Cross sections

## ABSTRACT

The  $\pi^+\pi^-$  photoproductions on the proton and deuteron have been studied in a photon energy range of 0.8–1.1 GeV at the Laboratory of Nuclear Science, Tohoku University. Charged pions and protons were detected using Neutral Kaon Spectrometer. We obtained the cross sections for the  $p(\gamma, p\pi^+\pi^-)$  and  $d(\gamma, p\pi^+\pi^-)n$ . The quasi-free process with a neutron spectator was extracted by the neutron momentum cut of  $p_n > 0.3$  GeV/c. The cross section for the  $\Delta^{++}\Delta^-$  production was deduced in the non-quasi-free process of the  $\gamma d \rightarrow pn\pi^+\pi^-$ . It was  $13.4 \pm 0.4$   $\mu\text{b}$  at  $E_\gamma = 0.82$  GeV.

© 2009 Elsevier B.V. Open access under [CC BY license](http://creativecommons.org/licenses/by/3.0/).

## 1. Introduction

Single and double pion photoproductions on the proton and deuteron have been investigated using large acceptance spectrometers and tagged photons [1–9]. In those studies, the double pion photoproductions were found to be approximately isospin-independent. Therefore, the photon-absorption cross section on the deuteron, which is about twice as large as that on the proton

[10–12], is understood as the sum of the contributions from the nucleons in the deuteron.

The cross section for the  $\gamma n \rightarrow n\pi^+\pi^-$  as well as that for the  $\gamma p \rightarrow p\pi^+\pi^-$  was also obtained using deuterium bubble chambers [13,14], where the “n” and “p” denote the neutron and proton in the deuteron. The results showed that the cross sections for the  $\pi^+\pi^-$  photoproduction on the “p” and “n” are nearly equal within the statistical uncertainties, and smaller than that on the free proton.

We must consider the contributions of the two-body photon absorption via meson exchange currents and a delta current in the case of the deuteron. Final state interactions also play an important role for the pion photoproductions. They were studied at the 1.3 GeV Tokyo electron synchrotron using the TAGX spectrometer [15], where the significant contribution of the  $\Delta^{++}\Delta^-$  excitation in the intermediate state was reported [16]. The cross section was calculated by Tejedor et al. [17], which reproduced the experimental data and predicted a sizable contribution of the double  $\Delta$  production above  $E_\gamma = 1$  GeV. They noted the importance of the detailed study in this energy region.

\* Corresponding author.

E-mail address: [hirose@lms.tohoku.ac.jp](mailto:hirose@lms.tohoku.ac.jp) (K. Hirose).<sup>1</sup> Laboratory of Nuclear Science, Tohoku University, Sendai 982-0826, Japan.<sup>2</sup> Department of Applied Biological Science, Tokyo University of Science, 2641 Yamazaki, Noda, Chiba 278, Japan.<sup>3</sup> Institute of Particle and Nuclear Studies, High Energy Accelerator Organization (KEK), Tsukuba 305-0801, Japan.<sup>4</sup> The Institute of Physical and Chemical Research (RIKEN), 2-1 Hirosawa, Wako, Saitama 351-0198, Japan.<sup>5</sup> Graduate School and undergraduate course, Physics Department, Gifu University, Yanagido, Gifu 501-1193, Japan.

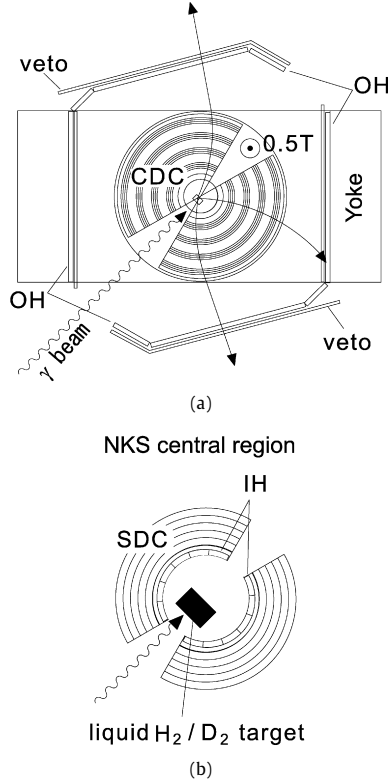


**Fig. 1.** (a) Top view of Neutral Kaon Spectrometer (NKS). It consists of a dipole magnet, hodoscopes (IH, OH), drift chambers (SDC, CDC), and veto counters (EV). (b) Closeup of the central region of NKS. The target is located inside IH.

In this Letter, we report the double pion photoproductions on the proton and deuteron. The cross section for the  $\gamma p \rightarrow p\pi^+\pi^-$ ,  $\gamma p \rightarrow p\pi^+\pi^-$  and the  $\gamma d \rightarrow \Delta^{++}\Delta^-$  was deduced.

## 2. Experimental procedure

The experiment was carried out at the Laboratory of Nuclear Science, Tohoku University. Electrons from a linear accelerator were injected into the Stretcher-Booster ring and accelerated up to 1.2 GeV. Bremsstrahlung photons were produced using an internal photon tagging system [18]. They impinged on the target after passing through a lead collimator with a length of 250 mm and a diameter of 10 mm placed 3.8 m downstream of a bremsstrahlung target. The photon energy was tagged in a range of 0.8–1.1 GeV using an array of plastic scintillators. The energy width of each counter was about 6 MeV. The typical tagging rate was 2 MHz. The tagging efficiency, which was periodically monitored during the experiment, was about 80% on average.

The liquid hydrogen and deuterium were used for the target. The target container was an aluminum cylinder 30 mm long and 50 mm in diameter. Both ends were covered with 75  $\mu\text{m}$  thick Upilex-S films [19]. It was located in the center of the spectrometer. The temperature of the target was automatically controlled and maintained at 14.5 K for the hydrogen and 19.1 K for the deuterium target. Their thicknesses were 254 and 571  $\text{mg}/\text{cm}^2$ , respectively.

Three charged particles in the final state were detected in coincidence using Neutral Kaon Spectrometer (NKS) [20,21]. As shown in Fig. 1, it consisted of two sets of drift chambers in a magnetic field, inner hodoscopes (IH) and outer hodoscopes (OH), and electron veto counters (EV). The magnetic field of 0.5 T was produced in the pole-gap space of 600 mm high and 1070 mm in diameter. The distribution of the magnetic field was calculated by the three-dimensional finite-element method program TOSCA. Timing

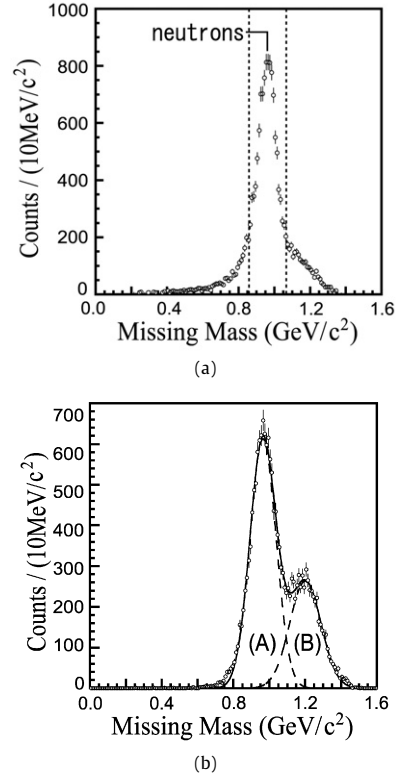


**Fig. 2.** (a) The missing mass distribution for the  $d(\gamma, p\pi^+\pi^-)X$  in the photon energy region of 0.96–1.00 GeV. The region between dashed lines is the cut for the  $d(\gamma, p\pi^+\pi^-)n$ . (b) The missing mass distribution for the  $d(\gamma, p\pi^-)X$ . It consists of two components as shown by the dashed lines. (A) and (B) are the contribution of the  $d(\gamma, p\pi^-)p$  and multi-pion productions, respectively.

signals from IH and OH were used for the trigger signals. The time-of-flight (TOF) was obtained from the time difference between IH and OH. The typical TOF resolution was  $\sigma = 0.5$  ns. A pair of the straw drift chambers (SDC) and cylindrical drift chambers (CDC) covered an angular range from  $\pm 10$  to  $\pm 170^\circ$  and from  $\pm 15$  to  $\pm 165^\circ$ , respectively. Pre-mixed gas of 50% argon and 50% ethane was supplied to the drift chambers. The spatial resolutions were about 0.5 mm for SDC and 0.4 mm for CDC. Together with the TOF resolution, they lead to a typical momentum resolution of 8% at 0.5 GeV/c.

The trigger signal for data acquisition (DAQ) was generated when at least one charged particle was detected on each arm of NKS along with one or more signals in the photon tagging system. The signals from EV were used as veto in the trigger. The DAQ efficiency was typically 90% at a trigger rate of 100 Hz.

## 3. Data analysis

The mass of the charged particles was calculated from the  $\beta$  and the momentum obtained from the SDC and CDC analysis. The proton contamination in the  $\pi^+$  selection and the  $\pi^+$  contamination in the proton selection were estimated to be less than 1.4% and 0.8%, respectively.

Fig. 2(a) shows the missing mass spectrum for the  $d(\gamma, p\pi^+\pi^-)X$ . The peak corresponding to the neutron mass is clearly seen. The dashed lines,  $\pm 2\sigma$  of the peak, are the cut for the  $d(\gamma, p\pi^+\pi^-)n$ . For the  $p(\gamma, p\pi^+\pi^-)X$ , the missing mass was calculated from two pions. The missing mass resolution was 34–65  $\text{MeV}/c^2$  at  $E_\gamma = 0.8$ –1.1 GeV. In the lowest photon energy region,  $E_\gamma = 0.81$ –0.83 GeV, the contamination from three or more pion production is negligibly small. According to Ref. [22], the upper value of the cross section for the  $\gamma p \rightarrow p\pi^+\pi^-\pi^0$  was about

4  $\mu\text{b}$  at  $E_\gamma = 0.8$  GeV. It is small compared with 75  $\mu\text{b}$  for the  $\gamma p \rightarrow p\pi^+\pi^-$  at the same photon energy. Therefore, the contamination in the higher photon energy region was estimated from this uncontaminated missing mass distribution and the energy dependence of the missing mass resolution. The contamination from  $3\pi$  productions was estimated to be less than 4%.

The  $d(\gamma, p\pi^-)p$  was analyzed for the consistency check. In the case of this reaction, there was a large background from double pion productions. In order to reduce them, we imposed cuts on the opening angle between the  $p$  and  $\pi^-$  ( $\cos \chi < 0.2$ ), and the angle of the  $p\pi^-$  system with respect to the beam direction ( $< 10^\circ$ ). These cuts lead to 40% loss of true events but 80% reduction of the background events. Fig. 2(b) shows the missing mass for the  $d(\gamma, p\pi^-)X$  after applying the cuts. The contamination from the multi-pion background was estimated to be 2–15% in the entire photon energy range.

Figs. 3(a) and 3(b) show the invariant mass distributions for the  $p\pi^\pm$  and  $\pi^+\pi^-$  pairs in the  $\gamma p \rightarrow p\pi^+\pi^-$  and  $\gamma^*p \rightarrow p\pi^+\pi^-$ , respectively. The  $\Delta^{++}\pi^-$  channel is a dominant process in this energy region as described in Refs. [22,23]. The peak around 1.35  $\text{GeV}/c^2$  in the  $p\pi^-$ -invariant mass distribution also corresponds to the  $\Delta^{++}\pi^-$  channel. The bump structure around 1.2  $\text{GeV}/c^2$  is thought to be the contribution from the  $\Delta^0\pi^+$  channel. Curves in the figures show the results of simulations described later. The dashed, dot-dashed, thick solid, and dotted curves show the invariant mass distributions for the  $\Delta^{++}\pi^-$ ,  $\Delta^0\pi^+$ ,  $p\rho^0$  channel, and the three-body-phase-space (3BPS) simulation, respectively. The thin solid curves are the sums of them.

The  $\gamma^*p \rightarrow p\pi^+\pi^-$  was derived according to the neutron momentum. Fig. 4 shows the neutron momentum distribution for the  $d(\gamma, p\pi^+\pi^-)n$ . The solid curve, calculated using the Hulthén wave function [24], corresponds to the nucleon momentum in the deuteron. The neutron momentum ( $p_n$ ) distribution can be represented by this curve when the  $p\pi^+\pi^-$ -final state is produced through the quasi-free (QF) process. We selected  $p_n < 0.2$   $\text{GeV}/c$  as the  $\gamma^*p \rightarrow p\pi^+\pi^-$  in which the neutron is the spectator. It should be noted that the QF process with the proton spectator is also possible. However, the momentum threshold of NKS, which is about 0.25  $\text{GeV}/c$  for protons, almost entirely precludes the detection of these events. We selected  $p_n > 0.3$   $\text{GeV}/c$  as the non-quasi-free (NQF) process in the  $\gamma d \rightarrow pn\pi^+\pi^-$ .

Fig. 5(a) shows the invariant mass distributions for the NQF kinematics in the  $d(\gamma, p\pi^+\pi^-)n$ . Not only the peak of the  $\Delta^{++}$  but also that of the  $\Delta^-$  can be seen. Curves show the results of the simulations. The dashed and dotted curves depict the invariant mass distributions for the  $\Delta^{++}\Delta^-$  channel and the four-body-phase-space (4BPS) simulation, respectively. In Fig. 5(b), the invariant mass distributions for the QF kinematics in the  $\gamma d \rightarrow pn\pi^+\pi^-$  are also shown for comparison. Clear differences can be seen according to the kinematical cut.

The acceptance of the spectrometer was estimated using GEANT4. Fig. 6 shows the Dalitz plot for the  $\gamma p \rightarrow p\pi^+\pi^-$  obtained from the 3BPS simulation at  $E_\gamma = 0.86$ – $0.90$  GeV. It is strongly distorted due to the acceptance restriction of NKS. This distortion, as a whole, makes a slight dip around the  $\Delta$  mass in the  $p\pi^\pm$ -invariant masses (the dotted curves in Fig. 3). It can also be seen that the peak-like structure around 0.3–0.4  $\text{GeV}/c^2$  in the  $\pi^+\pi^-$ -invariant mass is caused by the acceptance.

In the simulation, we considered  $\Delta^{++}\pi^-$ ,  $\Delta^0\pi^+$ ,  $p\rho^0$  and 3BPS as the channels for the  $\gamma p \rightarrow p\pi^+\pi^-$  and  $\gamma^*p \rightarrow p\pi^+\pi^-$ . The angular distributions of the  $\Delta^{++}$  production were taken from Ref. [22]. Since the angular distribution of the  $\Delta^{++}$  decay is roughly isotropic in the present photon energy region [22], it was approximated by a flat distribution. The angular distributions of the  $\Delta^0$  production and decay were treated in the same manner as in the  $\Delta^{++}\pi^-$  channel described above. For the  $\rho^0$  production

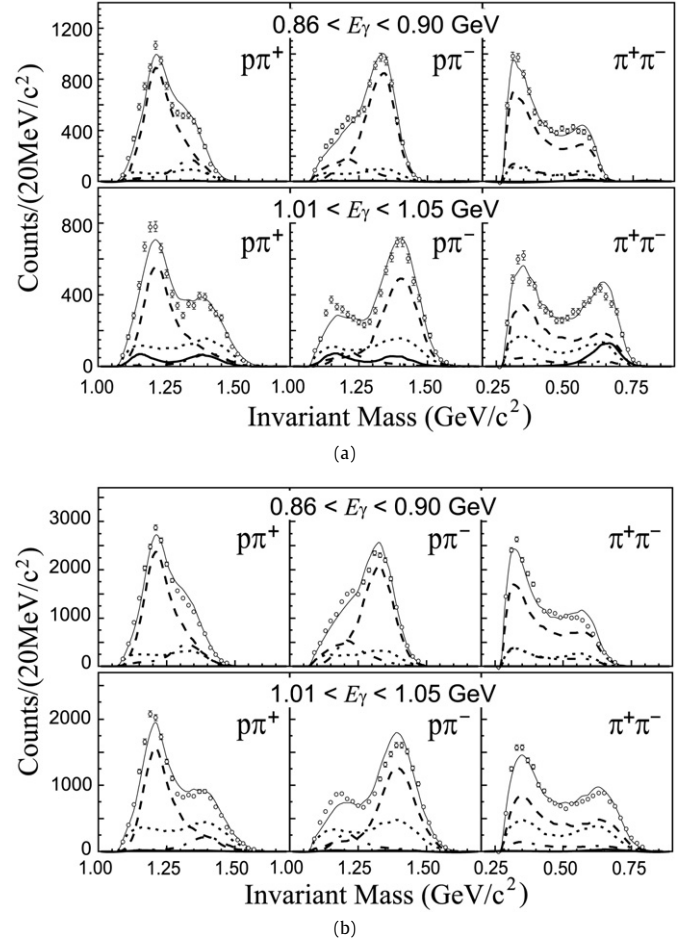


**Fig. 3.** Invariant mass distributions for (a) the  $\gamma p \rightarrow p\pi^+\pi^-$  and (b) the  $\gamma^*p \rightarrow p\pi^+\pi^-$  at two different photon energies. The selection method for the QF process is described in the text. Curves show the results of the simulations (see text). The dashed, dot-dashed, thick solid, and dotted curves represent the invariant mass distributions for the  $\Delta^{++}\pi^-$ ,  $\Delta^0\pi^+$ ,  $p\rho^0$  channel and the 3BPS simulation, respectively. The thin solid curves are the sums of them.

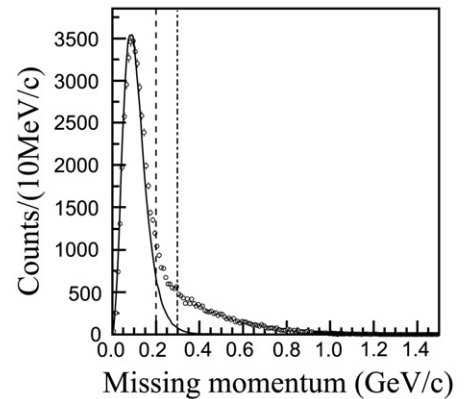


**Fig. 4.** The neutron momentum distribution for the  $d(\gamma, p\pi^+\pi^-)n$ . The solid curve indicates the momentum distribution of the nucleon in the deuteron.

channel, the forward peaking behavior of the angular distribution was taken into account. According to Ref. [23], the slope of its exponential behavior slightly decreases in the photon energy range between 1.4 and 2.6 GeV. The data measured at  $E_\gamma = 1.4$ – $1.6$  GeV were used for the angular distribution of the  $\rho^0$  production. We assumed an isotropic distribution for the  $\rho^0$  decay, since there are no measured data in the threshold region.

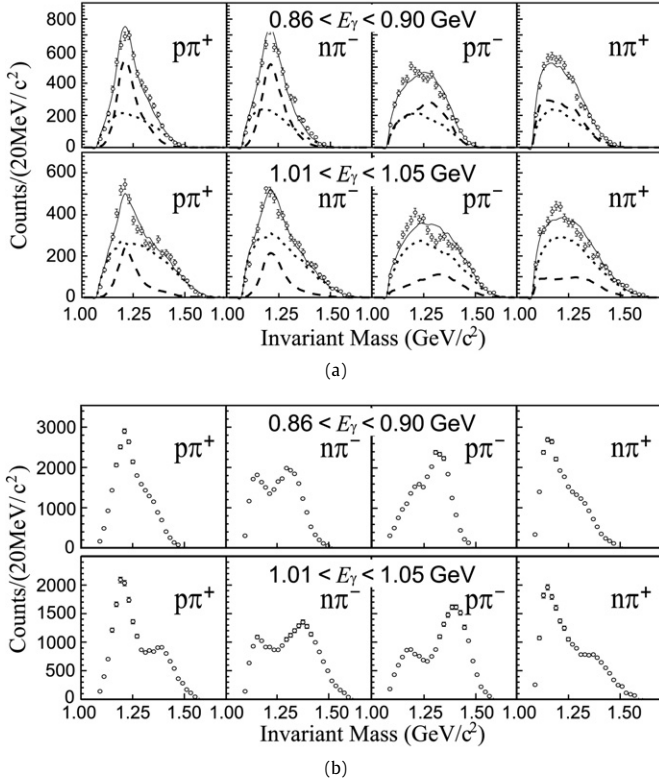


**Fig. 5.** (a) Invariant mass distributions for the NQF process ( $p_n > 0.3$  GeV/c) in the  $d(\gamma, p\pi^+\pi^-)n$  at two different photon energies. In this case, the peak of  $\Delta^-$  also appears. Curves show the results of the simulations (see text). The dashed and dotted curves depict the invariant mass distributions for the  $\Delta^{++}\Delta^-$  channel and the 4BPS simulation, respectively. The solid curves are their sums. (b) Invariant mass distributions for the QF process ( $p_n < 0.2$  GeV/c) in the  $d(\gamma, p\pi^+\pi^-)n$  at two different photon energies. They clearly differ from those in the NQF process.

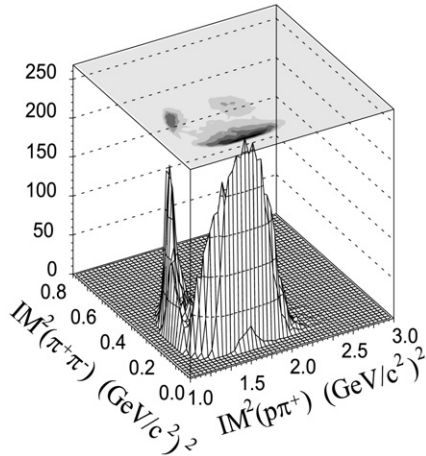


**Fig. 6.** The Dalitz plot for the  $\gamma p \rightarrow p\pi^+\pi^-$  obtained from the 3BPS simulation at  $E_\gamma = 0.86\text{--}0.90$  GeV.

For the deuteron target, the momenta of the proton and neutron were given according to the Hulthén wave function. For the NQF process in the  $\gamma d \rightarrow pn\pi^+\pi^-$ , the  $\Delta^{++}\Delta^-$  channel and 4BPS were taken into account. The  $\Delta^+\Delta^0$  channel will also contribute. As expected from the Clebsch–Gordan coefficients, the probability that the  $\Delta^+\Delta^0$  decays into  $pn\pi^+\pi^-$  is smaller by a factor of nine than that for the  $\Delta^{++}\Delta^-$ . Therefore, most parts of the  $\Delta^+\Delta^0$  decay contain at least one neutral pion. We excluded this channel from our consideration because it is undetectable in the present experiment.

The sums of the simulated invariant mass distributions were fitted to the experimental ones. The curves in Figs. 3 and 5(a) show the results of this fitting. The fractions of each channel were derived from this fitting. For example, the fraction of the  $\Delta^{++}\pi^-$  channel in the  $\gamma p \rightarrow p\pi^+\pi^-$  was given as

$$r_{(\Delta^{++}\pi^-)} = \frac{Y_{(\Delta^{++}\pi^-)}^{\text{sim}}}{Y_{(\Delta^{++}\pi^-)}^{\text{sim}} + Y_{(\Delta^0\pi^+)}^{\text{sim}} + Y_{(p\rho^0)}^{\text{sim}} + Y_{(3\text{BPS})}^{\text{sim}}}, \quad (1)$$

where  $Y^{\text{sim}}$  is the yield of each simulated channel. Assuming that the data can be reproduced by the combination of these channels, we can obtain the yield of the  $\Delta^{++}\pi^-$  channel by

$$Y_{(\Delta^{++}\pi^-)} = Y_{(p\pi^+\pi^-)} r_{(\Delta^{++}\pi^-)}, \quad (2)$$

where  $Y_{(p\pi^+\pi^-)}$  is the experimental yield of the  $\gamma p \rightarrow p\pi^+\pi^-$ .

#### 4. Results and discussion

The cross section for the  $i$ th channel was obtained by

$$\sigma_i = \frac{Y r_i}{N_T N_\gamma \varepsilon_{\text{DAQ}} \varepsilon_{\text{DC}}^n \varepsilon_{\text{track}}^n \eta_i}, \quad (3)$$

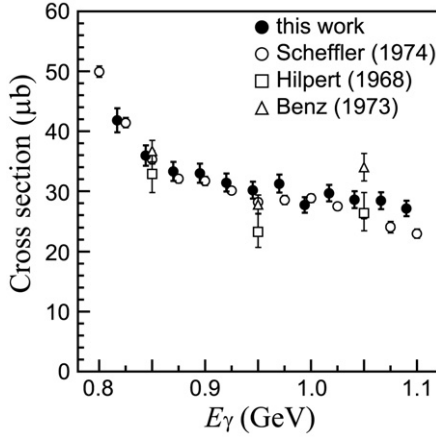
where  $N_T$  is the number of the target atoms per unit area,  $N_\gamma$  is the number of the incident photons,  $Y$  is the total yield,  $r_i$  is the fraction of the  $i$ th channel that was obtained using the invariant mass fittings in Figs. 3 and 5(a),  $\varepsilon_{\text{DAQ}}$  is the data-acquisition efficiency,  $\varepsilon_{\text{DC}}$  is the selection efficiency of track candidates, and  $\varepsilon_{\text{track}}$  is the tracking efficiency. The acceptance correction factor of the  $i$ th channel  $\eta_i$  was obtained using the simulation. It is given as the ratio of the number of accepted events to that of the generated ones. The typical values of  $\eta_i$  are 1.1% for the  $\gamma p \rightarrow \Delta^{++}\pi^-$  and  $\gamma^*p \rightarrow \Delta^{++}\pi^-$ , 1.2% for the  $\gamma p \rightarrow (p\pi^+\pi^-)_{3\text{BPS}}$  and  $\gamma^*p \rightarrow (p\pi^+\pi^-)_{3\text{BPS}}$ . The values for the free and QF process are almost same because of small kinematical effects of the Fermi motion. In the  $\Delta^{++}\Delta^-$  and 4BPS simulation, the efficiencies are estimated to be 0.4–0.6% in the entire photon energy range. The  $n$  is the number of the reconstructed tracks, e.g.  $n = 2$  for the  $\gamma^*n \rightarrow p\pi^-$ , and  $n = 3$  for the  $\gamma p \rightarrow p\pi^+\pi^-$  and  $\gamma d \rightarrow pn\pi^+\pi^-$ . The systematic uncertainties are estimated to be 4% for  $N_\gamma$ , 1% for  $\varepsilon_{\text{DAQ}}$ , 2% for  $\varepsilon_{\text{DC}}$  and 1% for  $\varepsilon_{\text{track}}$ . Most parts of the systematic uncertainties arise from the parameter  $r_i$  in the invariant mass fitting and the acceptance correction factor  $\eta_i$ . The total systematic uncertainty was estimated from the dispersion of the cross sections derived in several data taking periods. The cross section is given as the sum of the partial cross sections;  $\sigma_{\text{tot}} = \sum \sigma_i$ .

Fig. 7 shows the cross section for the  $\gamma^*n \rightarrow p\pi^-$ . This reaction has the simplest final state that can be measured using NKS. The acceptance for this reaction was calculated using the angular distributions of the  $\pi^-$  taken from Ref. [25]. Our data are compared to the previous works [25–27]. The statistical errors are shown. Our results are in good agreement with the previously obtained data.

The cross sections for the  $\gamma p \rightarrow p\pi^+\pi^-$  and  $\gamma p \rightarrow \Delta^{++}\pi^-$  are shown in Figs. 8(a) and 8(b), respectively. The error bars represent the statistical errors. The systematic uncertainty is estimated to be less than 6% for the  $\gamma p \rightarrow p\pi^+\pi^-$ , and to be less than 19% for the  $\gamma p \rightarrow \Delta^{++}\pi^-$ . These results are in agreement with those of ABBHHM [22] and SAPHIR [23]. The cross section for the  $\gamma p \rightarrow p\rho^0$  was found to begin to rise around 1 GeV and  $16.9 \pm 5.2$   $\mu\text{b}$  at  $E_\gamma = 1.1$  GeV. It is consistent with the previous results [22,23].

The cross section for the  $\gamma^*p \rightarrow p\pi^+\pi^-$  is shown in Fig. 9. The statistical errors are smaller than the symbols. The systematic uncertainty is estimated to be less than 8%. The results of previous works [13,14,16] are also shown for comparison. The data





**Fig. 7.** The cross section for the  $\gamma n \rightarrow p\pi^-$ . Closed circles show the results of this work. Open circles, open squares, and open triangles are the results of Scheffler [25], Hilpert [26] and Benz [27].

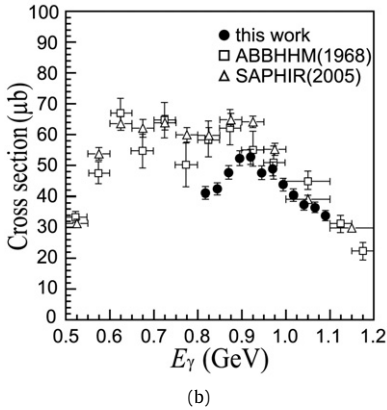
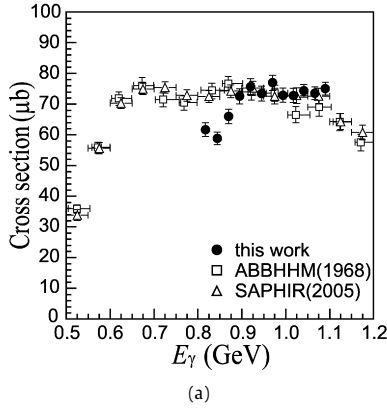


**Fig. 8.** The cross sections for (a) the  $\gamma p \rightarrow p\pi^+\pi^-$  and (b) the  $\gamma p \rightarrow \Delta^{++}\pi^-$ . Closed circles show the results of this work. Open squares and open triangles signify the results of ABBHHM [22] and SAPHIR [23].

of Refs. [13,14] were obtained using deuterium bubble chambers, and those of Ref. [16] were obtained using a magnetic spectrometer. The results of Refs. [14,16] are close to those for the  $\gamma p \rightarrow p\pi^+\pi^-$ , while our results show the continuity with the results of Ref. [13]. The cross section for the  $\pi^+\pi^-$  photoproduction on the bound proton is about half of that on the free proton.

Fig. 10 shows the cross section for the  $\gamma d \rightarrow \Delta^{++}\Delta^-$ . Closed circles show the results of this work. The statistical errors are smaller than the symbols. The systematic uncertainty is estimated to be less than 27%. For comparison, the results obtained in previous works [16,28,29] are also shown. The solid curve shows the calculation from Ref. [17]. In the present work, the cross section for

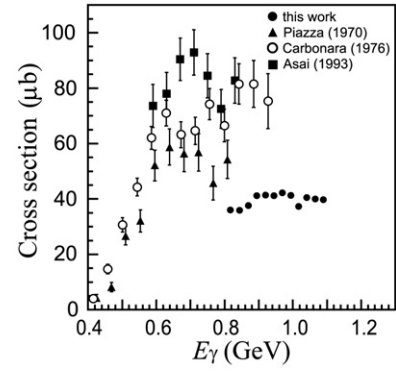


**Fig. 9.** The cross section for the  $\gamma p \rightarrow p\pi^+\pi^-$ . Closed circles represent the results of this work. Closed triangles, open circles, and closed squares show the results of Piazza [13], Carbonara [14] and Asai [16].

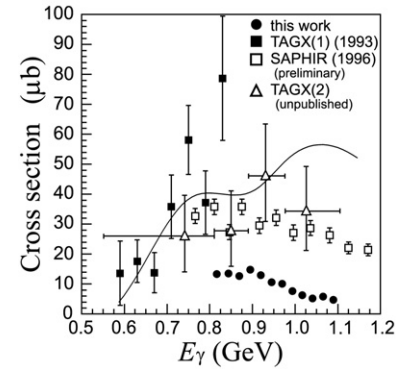


**Fig. 10.** The cross section for the  $\gamma d \rightarrow \Delta^{++}\Delta^-$ . Closed circles show the results of this work. Closed squares, open squares, and open triangles signify the results of TAGX(1) [16], SAPHIR [28], and TAGX(2) [29]. The solid curve shows the result of the calculation from Ref. [17].

the  $\gamma d \rightarrow \Delta^{++}\Delta^-$  is found to be smaller than those measured in the previous studies, and its energy dependence is different from the model prediction.

As mentioned above, the cross section for the bound proton is smaller than that for the free proton. The possible reason for the decrease of the cross section for the bound proton is thought to be final state interactions (FSI). For example, in the case of the  $\gamma d \rightarrow pn\pi^+\pi^-$ , the pion produced in the  $\gamma N \rightarrow \Delta\pi$  might interact with the spectator nucleon and the  $\pi N \rightarrow \Delta$  will occur when the pion has an appropriate momentum. If the QF production is followed by these FSIs, it will be identified as the NQF process in our data analysis. Therefore, the cross section for the bound nucleon apparently becomes smaller than that for the free nucleon. Consequently, the NQF cross section becomes larger.

It was reported that the influence of the Fermi motion on the cross section is small [8]. The DAPHNE result on the deuterium target corresponds to the sum of the contributions from the QF and NQF process, since the QF process was not distinguished from the NQF one in their analysis. In the present work, the sum of the cross sections for the QF and NQF process is  $64.4 \pm 5.6 \mu\text{b}$  at  $E_\gamma = 0.82 \text{ GeV}$ . Although this value is lower than the cross section for the  $\gamma p \rightarrow p\pi^+\pi^-$ , it is in agreement within  $2\sigma$  of the uncertainties. The present work shows the sizable contribution of the NQF process in the  $\pi^+\pi^-$  photoproduction on the deuteron, whereas this is not the case in the  $2\pi^0$  photoproduction [30].

## 5. Summary and conclusion

The cross sections have been measured for the  $\gamma p \rightarrow p\pi^+\pi^-$ ,  $\gamma p \rightarrow p\pi^+\pi^-$  and the NQF process in the  $\gamma d \rightarrow pn\pi^+\pi^-$  in

the photon energy range of 0.8–1.1 GeV. The cross section for the  $\gamma p \rightarrow p\pi^+\pi^-$  shows agreement with the previous data. The QF process was selected by applying the kinematical cut on the neutron momentum. The cross section for the  $\gamma p \rightarrow p\pi^+\pi^-$  was found to be smaller than that of the free proton.

The cross section for the  $\gamma d \rightarrow \Delta^{++}\Delta^-$  was measured. It was found to be smaller than the previous data and showed decreasing behavior with the photon energy. A model adapted to this energy region is needed for more detailed investigation of the double  $\Delta$  excitation.

### Acknowledgements

We would like to thank the accelerator and technical staff at the Laboratory of Nuclear Science for operation of the accelerator and for other experimental supports. This work was supported by a Grant-in-Aid for Scientific Research from The Ministry of Education, Culture, Sports and Technology, Japan, Nos. 09304028, 12002001 and 14740150.

### References

- [1] A. Braghieri, et al., Phys. Lett. B 363 (1995) 46.
- [2] F. Härter, et al., Phys. Lett. B 401 (1997) 229.
- [3] M. Wolf, et al., Eur. Phys. J. A 9 (2000) 5.
- [4] J. Ahrens, et al., Phys. Lett. B 624 (2005) 173.
- [5] B. Krusche, et al., Eur. Phys. J. A 6 (1999) 309.
- [6] V. Kleber, et al., Eur. Phys. J. A 9 (2000) 1.
- [7] W. Langgärtner, et al., Phys. Rev. Lett. 87 (2001) 052001.
- [8] A. Zabrodin, et al., Phys. Rev. C 55 (1997) R1617.
- [9] A. Zabrodin, et al., Phys. Rev. C 60 (1999) 055201.
- [10] T.A. Armstrong, et al., Phys. Rev. D 5 (1972) 1640.
- [11] T.A. Armstrong, et al., Nucl. Phys. B 41 (1972) 445.
- [12] M. McCormick, et al., Phys. Rev. C 53 (1996) 41.
- [13] A. Piazza, et al., Nuovo Cimento 3 (1970) 403.
- [14] F. Carbonara, et al., Nuovo Cimento A 36 (1976) 219.
- [15] K. Maruyama, et al., Nucl. Instrum. Methods A 376 (1996) 335.
- [16] M. Asai, et al., Z. Phys. A 344 (1993) 335.
- [17] J.A. Gómez Tejedor, E. Oset, H. Toki, Phys. Lett. B 346 (1995) 240.
- [18] H. Yamazaki, et al., Nucl. Instrum. Methods A 536 (2005) 70.
- [19] Ube Ultra-High Heat-Resistant Polyimide Film, Ube Industries Ltd., 2000.
- [20] T. Watanabe, et al., Phys. Lett. B 651 (2007) 269.
- [21] K. Tsukada, et al., Phys. Rev. C 78 (2008) 014001.
- [22] ABBHHM Collaboration, Phys. Rev. 175 (1968) 1669.
- [23] C. Wu, et al., Eur. Phys. J. A 23 (2005) 317.
- [24] D.H. White, R.M. Schectman, B.M. Chasan, Phys. Rev. 120 (1960) 614.
- [25] P.E. Scheffler, P.L. Walden, Nucl. Phys. B 75 (1974) 125.
- [26] H.G. Hilpert, et al., Nucl. Phys. B 8 (1968) 535.
- [27] P. Benz, et al., Nucl. Phys. B 65 (1973) 158.
- [28] Y. Wada, for the SAPHIR Collaboration, Particles and nuclei international conference, Williamsburg, Virginia, 1996.
- [29] A. Shinozaki, for the TAGX Collaboration, private communication.
- [30] J. Ajaka, et al., Phys. Lett. B 651 (2007) 108.